IEEE Photonics Journal
An IEEE Photonics Society Publication

Open Access

Transmissive Refractive Index Sensing Based on Frequency-Sensitive Responses of Two-Dimensional Photonic Crystals

Volume 8, Number 5, October 2016

Xulin Lin
Haiwen Fang
Lin Wang
Guo Ping Wang
Xunya Jiang

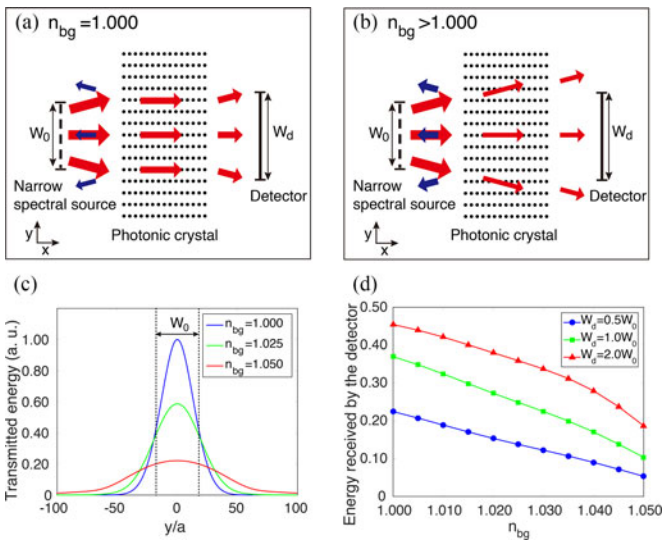

DOI: 10.1109/JPHOT.2016.2615283
1943-0655 © 2016 IEEE

IEEE photonics SOCIETY

IEEE

Transmissive Refractive Index Sensing Based on Frequency-Sensitive Responses of Two-Dimensional Photonic Crystals

Xulin Lin,[1] Haiwen Fang,[2, 3] Lin Wang,[4] Guo Ping Wang,[1] and Xunya Jiang[2, 3]

[1]College of Electronic Science and Technology, Guangdong Provincial Key Laboratory of Micro/Nano Optomechatronics Engineering, and Key Laboratory of Optoelectronic Devices and Systems of Ministry of Education and Guangdong Province, Shenzhen University, Shenzhen, 518060, China
[2]Department of Illuminating Engineering and Light Sources, School of Information Science and Engineering, Fudan University, Shanghai, 200433, China
[3]Engineering Research Center of Advanced Lighting Technology, Fudan University, Ministry of Education, Shanghai, 200433, China
[4]State Key Laboratory of Functional Materials for Informatics, Shanghai Institute of Microsystem and Information Technology, Chinese Academy of Sciences, Shanghai 200050, China

DOI:10.1109/JPHOT.2016.2615283

Manuscript received September 14, 2016; revised September 30, 2016; accepted October 2, 2016. Date of publication October 5, 2016; date of current version October 20, 2016. This work was supported in part by NKBRPC under Grant 2012CB927401; in part by the National Natural Science Foundation of China under Grant 11274247, Grant 11574218, Grant 11504243, Grant 11604217, Grant 61475180, Grant 11334015, and Grant 11204340; in part the Natural Science Foundation of Guangdong Province, China, under Grant 2016A030313042 and Grant 2015A030310400, and in part by the STCSM under Grant 14JC1407600. Corresponding authors: G. P. Wang and X. Jiang (e-mail: gpwang@szu.edu.cn; jiangxunya@fudan.edu.cn).

Abstract: In this paper, we propose a new scheme of refractive index (RI) sensing, which utilizes frequency-sensitive responses of 2-D photonic crystals. Specifically, the 2-D photonics crystals consist of dielectric rods arranged in rectangular lattice and support frequency-sensitive supercollimation (SC). Small changes in ambient RI are sensed by measuring transmission rate of a narrow spectral source. This RI sensing scheme exploits the sensitive dispersion properties around the SC frequency: Both reflection and beam diffraction are enhanced in response to a slight increase of ambient RI. Operation and performance of the transmissive RI sensing are demonstrated by finite-difference time-domain (FDTD) simulations. The major advantage of our design is that all the essential components can be compactly integrated, which makes it attractive for a number of applications, such as hand-held equipment and distributed sensor networks.

Index Terms: Photonic crystal, sensors.

1. Introduction

Refractive index (RI) sensors, which transduce small RI changes into observable optical signals, are useful for many applications, such as bio-chemical analysis and environmental monitoring [1]–[3]. Most of the high performance RI sensors are based on micro-cavities supporting high-Q resonant

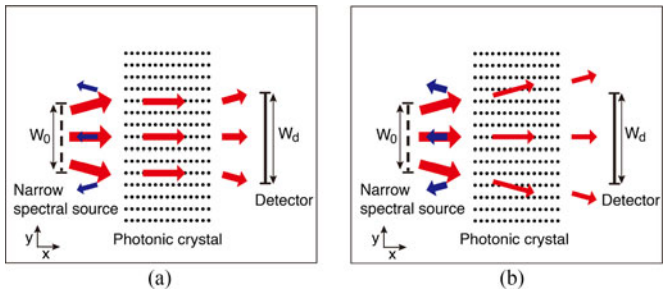

Fig. 1. Schematics of the transmissive RI sensing. A narrow spectral source is normally launched into a PhC consisting of dielectric rods arranged in rectangular lattice, and the central part of the transmitted light energy is received by a detector. When the ambient RI $n_{bg} = 1.000$, the light beam is collimated inside the PhC. With small increase of n_{bg}, both diffraction and reflection are enhanced, thus resulting in significant reduction in light energy received by the detector. (a) $n_{bg} = 1.000$. (b) $n_{bg} > 1.000$.

modes, and variations of RI within the cavity area are determined by measuring shifts of the resonant frequencies [4]–[7]. However, it is worth noting that although the micro-cavities can be fabricated in a chip with minimum sizes, the optical spectrum analyzers (OSAs) used to track movements of the resonant frequencies are bulky and expensive, thus making these resonant RI sensor unsuitable in some applications, such as handheld equipments and distributed sensor networks.

In this paper, we propose an alternative scheme of RI sensing based on frequency-sensitive responses of defect-free photonic crystals (PhCs), in which small variations of ambient RI are sensed by measuring transmission of a narrow spectral light source. Specifically, the frequency-sensitive responses we make use of arise from the frequency-sensitive supercollimation (FSSC) phenomenon [8]–[10] supported by 2-D rectangular lattice PhCs consisting of dielectric rods. FSSC means that around the flat equi-frequency-contour (EFC) representing supercollimation (or self-collimation, both short for SC) [11]–[14], EFC curvature changes dramatically with respect to frequency due to small group velocities [8]. The basic setup of the transmissive RI sensing is schematically shown in Fig. 1. A narrow spectral source with central frequency around the SC frequency is normally launched into the PhC. With small increases of ambient RI n_{bg}, both reflection and diffraction (transversally broadness) are enhanced due to enlarged EFC curvature and reduced group velocity, respectively, which together result in significantly reduction in transmitted light energy received by the detector of finite spatial extent. Therefore small variations of n_{bg} can be determined by measuring the transmitted light energy. By avoiding using the bulky OSAs, all the essential components in our transmissive RI sensing scheme can be compactly integrated. Moreover, the measurement of light energy is much faster than tracking the movement of resonant frequencies.

The organization of this article is as follows. In Section 2, we validate our design by analyzing variations of the dispersion properties around the SC frequency in response to small changes of ambient RI. In Section 3, we demonstrate operation and performance of the transmissive RI sensing by finite-difference time-domain (FDTD) simulations. In Section 4, we discuss the influence of weak disorder of the PhC to performance of the transmissive RI sensing.

2. Principle of the Transmissive RI Sensing

We first analyze variations of the dispersion properties around the SC frequency in response to small variations of ambient RI. The 2-D PhC we consider consists of dielectric rods arranged in rectangular lattice [see the inset of Fig. 2(b)]. Radius of the rods is $r = 0.35a$ and the aspect ratio of the rectangular lattice is $\beta = b/a = 2.0$, where a and b are lattice units in x and y direction, respectively. RI of the dielectric material is $n = 3.4$. RI in space between the rods is denoted as n_{bg}. Dispersion relations $\omega(\mathbf{k})$ of the PhC are computed using FDTD simulations with Bloch boundary conditions [15], [16]. Fig. 2(a) shows the characteristic EFC distribution of FSSC in the second TE (electric field in xy plane) band when $n_{bg} = 1.000$. SC is represented by the flat EFC line corresponding to $\omega_0 = 0.3455(2\pi c/a)$; with the flat EFC, light of frequency ω_0 is collimated along x

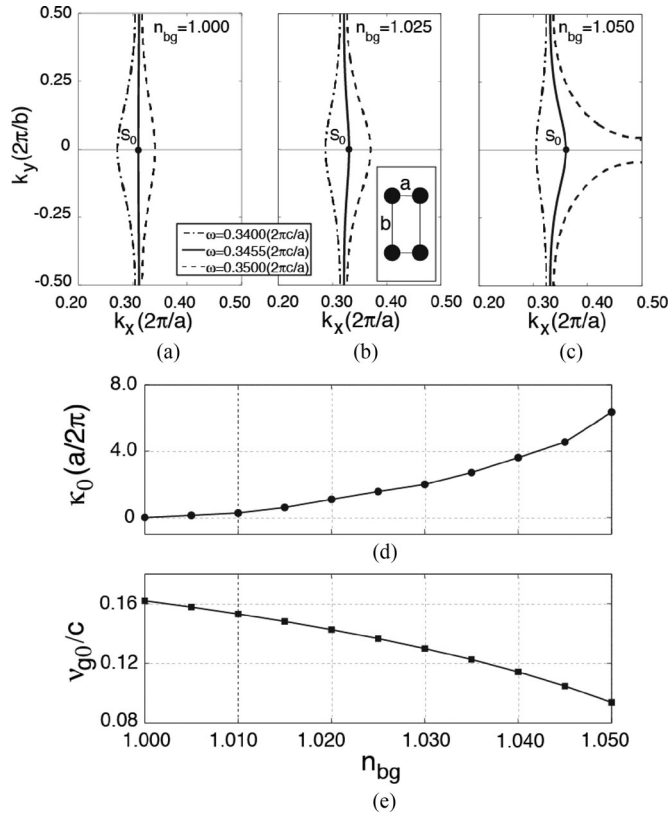

Fig. 2. Analysis of the dispersion properties around the SC frequency in response to small changes of ambient RI n_{bg}. (a) Characteristic EFC distribution of FSSC when $n_{bg} = 1.000$. (b) and (c) Deformations of the EFC distribution when $n_{bg} = 1.025$ and $n_{bg} = 1.050$, respectively. (d) and (e) Tendencies of EFC curvature κ_0 and group velocity v_{g0} at the S_0 point with respect to n_{bg}, respectively.

direction inside the PhC [11], [12]. Around the flat EFC, the EFCs with small frequency differences (approximately $\pm 0.015\omega_0$) are curved around the k_x axis, thus indicating the SC is very sensitive to frequency changes [8].

The fact that SC is frequency sensitive also indicates that dispersion properties around the SC frequency is sensitive to RI changes. Here, we pay special attention to the center point of the ω_0 EFC S_0. Group velocity and EFC curvature at the S_0 point are calculated according to [10], [17]

$$v_{g0} = \frac{\partial \omega}{\partial k_x}|_{k_y=0,\omega=\omega_0} \tag{1}$$

and

$$\kappa_0 = \frac{\partial^2 \omega}{\partial k_y^2} \Big/ \frac{\partial \omega}{\partial k_x}|_{k_y=0,\omega=\omega_0}. \tag{2}$$

Tendencies of the EFC curvature κ_0 and the group velocity v_{g0} with respect to n_{bg} are show in Fig. 2(d) and (e), respectively. As can be seen, when n_{bg} changes from 1.000 to 1.050, κ_0 increases from 0 to $6.7(a/2\pi)$, and v_{g0} decreases from $0.16c$ to $0.09c$, where c is the speed of light in a vacuum.

Implications of increasing κ_0 and of decreasing v_{g0} to light propagation are explained as follows. For a light beam launched in x direction and of frequency ω_0, the EFC curvature κ_0 determines beam diffraction (transversal broadness). Zero κ_0 means beam diffraction is totally suppressed, i.e., beam width is frozen when propagating inside the PhC. With $\kappa_0 > 0$, the beam expands transversally

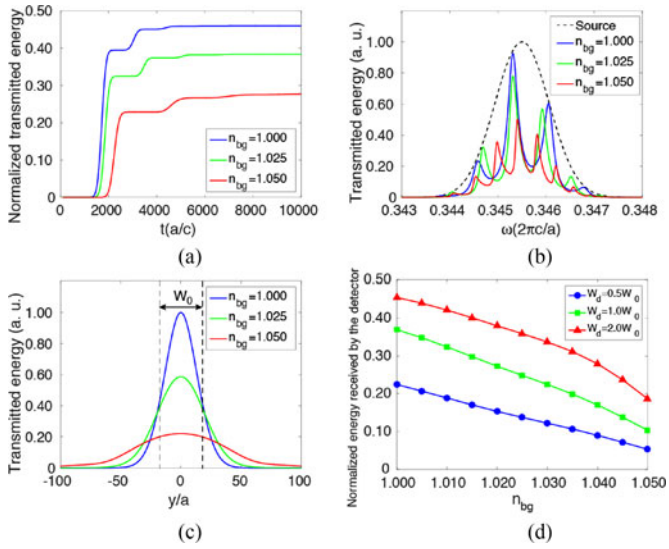

Fig. 3. Operation and performance of the transmissive RI sensing using PhC with perfect periodicity. (a) Time evolutions of accumulated transmitted light energy integrated over the whole detector plane. The values of transmitted light energy are normalized to total energy of the narrow spectral pulsed source. (b) Spectra of the total transmitted energy. The black dashed line shows spectrum of the pulsed source. (c) Spatial distributions of the total transmitted energy. W_0 is the initial spatial width of the pulsed source. (d) Relations between ambient RI n_{bg} and light energy received by the detector. Three different detector widths W_d are assumed.

during propagation inside the PhC. On the other hand, the decreasing group velocity v_{g0} not only slows down the speed of light propagation inside the PhC but also enhances reflection on the boundaries of the PhC due to more severe impedance mismatching [18]–[20].

The above analysis validates the principle of our RI sensing scheme shown in Fig. 1. For a narrow spectral source with central frequency of ω_0 and launched in x direction, which couples to a small region around the S_0 point, both reflection and diffraction are enhanced with small increases of n_{bg}, and the transmitted light energy received by the detector is reduced as a result. Due to the monotonous relation between n_{bg} and the transmitted light received by the detector, an unknown n_{bg} can be determined by measuring the transmitted light after a calibrating process.

3. Operation and Performance of the Transmissive RI Sensing

We next demonstrate operation and performance of the transmissive RI sensing based on FSSC by FDTD simulations. The size of the PhC is $100a \times 100b$. A narrow-spectral pulsed source with finite spatial extent is launched from the left side of the PhC, which is defined by H_z (z component of magnetic field) distribution $10a$ from the left side of the PhC:

$$H_z(y, t) = H_{z0}\exp(-y^2/2W_0^2)\exp[-i\omega_0 t - (t - 2\tau_0)^2/\tau_0^2], \tag{3}$$

where $W_0 = 36a$ is the initial spatial width of the incident pulse, and $\tau_0 = 200(a/c)$ is the temporal width of the pulse. The detector used to receive central part of the transmitted light energy is placed $10a$ from the right side of the PhC, with the width denoted as W_d. Simulations are repeated for n_{bg} from 1.000 to 1.050 in step of 0.005. During each simulation, we record electromagnetic fields on the detector plane at every time step. These data are then used to analyze time evolutions, spectra, and spatial distributions of the transmitted light energy.

Fig. 3(a) shows time evolutions of accumulated transmitted light energy integrated over the whole detector plane, in which we can see that the incident pulse experiences a multi-reflection process before totally transmitting though the PhC. The interval between two neighboring rises of the time-

accumulated transmitted energy corresponds to the time needed for the pulse to travel a round-trip inside the PhC. As can be seen in Fig. 3(a), the time-accumulated transmitted energy become stable within several round-trips, indicating the incident pulse totally transmits through the PhC within a very short time.

Fig. 3(b) shows spectra of the total transmitted energy for different values of n_{bg}. The spectrum of the incident pulse is also provided for comparison. Due to the multiple-reflection process, there are a bunch of fringes in the transmission spectra caused by Fabry-Perot (FP) interference. Spectral distances of the neighboring fringes (known as free spectral ranges) for larger n_{bg} are narrower due to reduced group velocities [21]. Previously, it was demonstrated that RI changes can be sensed by monitoring variations of free spectral ranges [22]. However, such method requires precise analysis of the transmission spectra, and the use of bulky and expensive OSAs is required. On the other hand, although single-frequency transmission rates are strongly modulated by the FP fringes, the multi-frequency transmitted energy integrated over several free spectral ranges changes monotonically and smoothly with respect to n_{bg}, as will be shown latter.

The effects of simultaneously enhanced diffraction and reflection with increasing n_{bg} can be seen in the spatial distributions of transmitted light energy, as shown in Fig. 3(c). With increase of n_{bg}, the total transmitted energy is reduced as a result of enhanced reflection, and the spatial distribution becomes flatter due to enhanced diffraction. These results verify our analysis of the dispersion properties around the S_0 point.

We next analyze the relation between n_{bg} and transmitted energy received by the detector. Three different detector widths are supposed: $W_d = 0.5W_0$, $W_d = 1.0W_0$, and $W_d = 2.0W_0$, where $W_0 = 36a$ is the initial spatial width of the incident pulse. As shown by Fig. 3(d), for all the three cases, energy received by the detector drops monotonically and smoothly as n_{bg} increases from 1.000 to 1.050. Therefore $n_{bg} \in [1.000, 1.050]$ can be uniquely determined by measuring the transmitted light energy. Data shown in Fig. 3(d) are normalized by total energy of the pulsed source. Compared to the corresponding values when $n_{bg} = 1.000$, energy received by the detector when $n_{bg} = 1.050$ reduced by 76% for $W_d = 0.5W_0$, by 72% for $W_d = 1.0W_0$, and by 59% for $W_d = 2.0W_0$. The different relative sensitivities of received energy with respect to n_{bg} is attributed to different contributions of diffraction: diffraction means that light energy spreads transversally, and reduction in received transmitted energy due to enhanced diffraction is more significant for narrower detector width. Resolution of the transmissive RI sensing (minimum detectable Δn_{bg}) is determined by a number of factors, including slope of the characteristic line (relation between n_{bg} and transmitted energy received by the detector), intensity and stability of the narrow spectral source, and accuracy of the measurement of light energy. For example, for the case of $W_d = 1.0W_0$, suppose that the uncertainty due to source instability and light energy measurement is 0.1% of the total launched energy; then, the minimum detectable Δn_{bg} is estimated to be 3.8×10^{-3}RIU.

4. Influence of Weak Disorder of the PhC

We finally discuss influence of weak disorder of the PhC to performance of the transmissive RI sensing. In the above, we suppose that the PhC is composed by dielectric rods with uniform size and arranged in perfectly periodic lattice. However, some amount of weak disorder due to fabrication inaccuracy is inevitable for real PhCs. It is therefore of importance to discuss how the inherently weak disorder imposed to the PhC influences performance of the transmissive RI sensing. We assume that weak disorder of the PhC is solely attributed to small randomness of radii of the dielectric rods Δr. This assumption is justified by the fact that patterns of PhCs can precisely defined by interference lithography, while actual shapes of the unit cells may deviate from the design in fabricating process [23]–[25]. Deviations of rod shape from circular are omitted for simplicity of discussion. Here we consider three configurations with different magnitudes of randomness. Root-mean-square of Δr for these configurations are $\Delta r_{\text{rms}} = 5.0 \times 10^{-4}a$, $\Delta r_{\text{rms}} = 1.0 \times 10^{-3}a$, and $\Delta r_{\text{rms}} = 2.0 \times 10^{-3}a$.

In Fig. 4(a), we compare the spatial distributions of transmitted energy of the weakly disordered PhCs to that of the periodic PhC when $n_{bg} = 1.025$. For the weakly disordered PhCs, we can

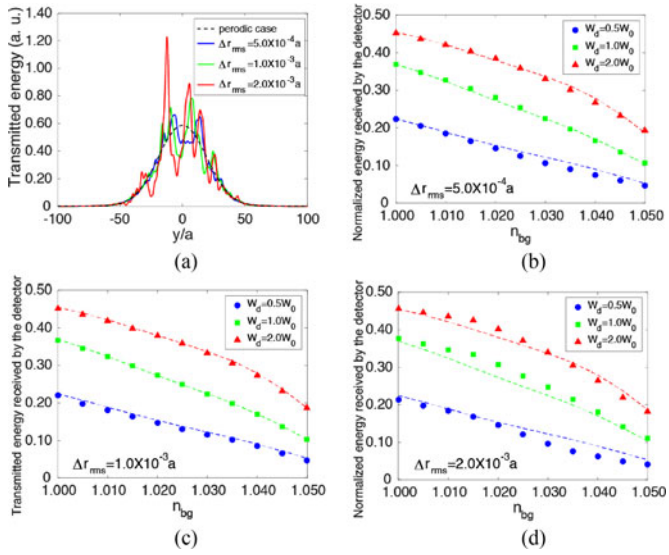

Fig. 4. Influence of weak disorder of the PhC to the performance of the transmissive RI sensing. Δr_{rms} is the root mean square error of radii of the dielectric rods that compose the PhC. (a) Spatial distributions of transmitted energy for the weakly disordered PhCs when $n_{bg} = 1.025$. The black dashed line corresponds to the PhC with perfect periodicity. (b)–(d) Relations between ambient RI n_{bg} and light energy received by the detector for the weakly disordered PhCs with different magnitudes of disorder. The dashed lines show the corresponding values for the periodic PhC.

see irregular fluctuations caused by multiple random scattering inside the PhC, and magnitudes of the fluctuations are correlated to magnitude of Δr_{rms}: Stronger disorder results in more intense fluctuations. In Fig. 4(b)–(d), we show relations between n_{bg} and transmitted light energy received by the detector for the PhCs imposed with weak disorder. The corresponding data for the periodic PhC (represented by dashed lines) are also provided for comparison. For the configuration with $\Delta r_{\text{rms}} = 5.0 \times 10^{-4}a$ and $\Delta r_{\text{rms}} = 1.0 \times 10^{-3}a$ [see Fig. 4(b) and (c)], values of the received light energy are very close to those of the periodic PhC, thus indicating the fluctuations of transmitted light caused by multiple random scattering are generally smoothed out within the spatial range of the detector. For the configuration with $\Delta r_{\text{rms}} = 2.0 \times 10^{-3}a$ [see Fig. 4(d)], however, values of the received light energy deviate obviously from those of the periodic PhC. Such deviation means the performance of RI sensing is severely degraded, as the multiple random scattering imposes significant uncertainty in the relation between n_{bg} and light energy received by the detector. Therefore, we assert that weak disorder imposed to the PhC influences performance of the transmissive RI sensing in a "threshold" manner: There exists a critical degree of disorder below which performance of the transmissive RI sensing is robust against random multiple scattering caused by disorder.

5. Conclusion

In conclusion, we numerically show that by utilizing FSSC supported by 2D PhCs consisting of dielectric rods, small changes of ambient RI can be sensed by measuring transmitted energy of a narrow spectral source. Our transmissive RI sensing scheme exploits the frequency-sensitive response around the SC frequency. Both diffraction and reflection are enhanced in response to small increases of ambient RI, and the transmitted light energy received by a detector with spatial extent comparable to the source width is significantly reduced as a result. For the specific configuration of photonic crystals we consider in this article, the received light energy drops by more than 50% when the ambient RI changes from 1.000 to 1.050. As revealed in our previous work [8], frequency sensitivity of SC can be tuned over a wide range. Therefore, sensitivity and measurable range of the transmissive RI sensing can be changed by adjusting parameters of the PhC. Narrow spectral

source are used in the purpose of smoothing out the spectral fringes caused by FP interference. In our FDTD simulations, we assume the narrow spectral source to be a pulse with a approximately 1% spectral width with respect to the central frequency. It is worth noting that, however, use of pulsed laser sources is not necessary. Practically, the pulsed source can be replaced by a more compact superluminescent diode [26], which emits continuous light over a narrow spectral range, and small changes of ambient RI can be sensed by measuring the stable transmitted intensity instead of time-accumulated transmitted energy. We also note that for real applications, the 2-D PhC, which is a simplified theoretical model composed by infinitely long dielectric rods, should be replaced by a PhC slab consisting of dielectric rods of finite thickness and supported by low index substrate. In that case, all the essential components required to implement the transmissive RI sensing can be compactly integrated, thus making our design attractive for handheld equipment and distributed sensor networks.

References

[1] R. V. Nair and R. Vijaya, "Photonic crystal sensors: an overview," *Prog. Quantum Electron.*, vol. 34, pp. 89–134, 2010.
[2] X. Fan, I. M. White, S. I. Shopova, H. Zhu, J. D. Suter, and Y. Sun, "Sensitive optical biosensors for unlabeled targets: a review," *Anal. Chim. Acta*., vol. 620, pp. 8–26, 2008.
[3] X. Fan and I. M. White, "Optofluidic microsystems for chemical and biological analysis," *Nat. Photon*., vol. 5, pp. 591–597, 2011.
[4] T. Sünner *et al*., "Photonic crystal cavity based gas sensor," *Appl. Phys. Lett*,. vol. 92, 2008, Art. no. 261112.
[5] D. F. Dorfner, T. Hürlimann, T. Zabel, L. H. Frandsen, G. Abstreiter, and J. J. Finley, "Silicon photonic crystal nanostructures for refractive index sensing," *Appl. Phys. Lett*., vol. 93, 2008, Art. no. 181103.
[6] A. Falco, L. O'Faolain, and T. F. Krauss, "Chemical sensing in slotted photonic crystal heterostructure cavities," *Appl. Phys. Lett*., vol. 94, 2009, Art. no. 063503.
[7] I. M. White and X. Fan, "On the performance quantification of resonant refractive index sensors," *Opt. Exp*., vol. 16, pp. 1020–1028, 2008.
[8] X. Lin, X. Zhang, L. Chen, M. Soljačić, and X. Jiang, "Super-collimation with high frequency sensitivity in 2D photonic crystals induced by saddle-type van Hove singularities," *Opt. Exp*., vol. 21, pp. 30140–30147, 2013.
[9] W. Li, X. Zhang, X. Lin, and X. Jiang, "Enhanced wavelength sensitivity of the self-collimation superprism effect in photonic crystals via slow light," *Opt. Lett*., vol. 39, 4486–4489, 2014.
[10] X. Lin, X. Zhang, K. Yao, and X. Jiang, "Wide-range and tunable diffraction management using 2D rectangular lattice photonic crystals," *J. Opt. Amer. B*, vol. 31, pp. 1145–1149, 2014.
[11] H. Kosaka *et al*., "Self-collimating phenomena in photonic crystals," *Appl. Phys. Lett*., vol. 74, pp. 1212–1214, 1999.
[12] J. Witzens, M. Loncar, and A. Scherer, "Self-collimation in planar photonic crystals," *IEEE J. Sel. Topics Quantum Electron*., vol. 8, pp. 1246–1257, 2002.
[13] D. Zhao, J. Zhang, P. Yao, X. Jiang, and X. Chen, "Photonic crystal mach-zehnder interferometer based on self-collimation," *Appl. Phys. Lett*., vol. 90, 2007, Art. no. 231114.
[14] H. Li *et al*., "Millimeter-scale and large-angle self-collimation in a photonic crystal composed of silicon nanorods," *IEEE Photon. J*., vol. 5, Apr. 2013, Art. no. 2201306.
[15] A. Taflove and S. C. Hagness, *Computational Electrodynamics: The Finite-Difference Time-Domain Method*, 3rd ed. Norwood, MA, USA: Artech House, 2005.
[16] A. F. Oskooi, D. Roundy, M. Ibanescu, P. Bermel, J. D. Joannopoulos, and S. G. Johnson, "MEEP: A flexible free-software package for electromagnetic simulations by the FDTD method," *Comput. Phys. Commun*., vol. 181, pp. 687–702, 2010.
[17] M. J. Steel *et al*., "Analytic properties of photonic crystal superprism parameters," *Phys. Rev. E*, vol. 71, no. 5 pt. 2, 2005, Art. no. 056608.
[18] Y. A. Vlasov and S. J. McNab, "Coupling into the slow light mode in slab-type photonic crystal waveguides," *Opt. Lett*., vol. 31, pp. 50–52, 2006.
[19] C. M. de Sterke, J. Walker, K. B. Dossou, and L. C. Botten, "Efficient slow light coupling into photonic crystals," *Opt. Exp*., vol. 15, pp. 10984–10990, 2007.
[20] T. BaBa, "Slow light in photonic crystals," *Nat. Photon*., vol. 2, pp. 465–473, 2008.
[21] M. Born and E. Wolf, *Principle of Optics—Electromagnetic Theory and Propagation*, 7th ed. Cambridge, U.K.: Cambridge Univ. Press, 1999.
[22] V. S. Y. Lin, K. Motesharei, K. P. S. Dancil, M. J. Sailor, and M. R. Ghadiri, "A porous silicon-based optical interferometric biosensor," *Science*, vol. 278, pp. 840–843, 1997.
[23] P. T. Rakich *et al*., "Achieving centimetre-scale supercollimation in a large-area two-dimensional photonic crystal," *Nat. Mater*., vol. 5, pp. 93–96, 2006.
[24] J. Lee, B. Zhen, S.-L. Chua, O. Shapira, and M. Soljačić, "Fabricating centimeter-scale high quality factor two-dimensional periodic photonic crystal slabs," *Opt. Exp*., vol. 22, pp. 3724–3731, 2014.
[25] S. Behera, M. Kumar, and J. Joseph, "Submicrometer photonic structure fabrication by phase spatial-light-modulator-based interference lithography," *Opt. Lett*., vol. 41, pp. 1893–1896, 2016.
[26] L. H. Li, M. Rossetti, A. Fiore, L. Occhi, and C. Velez, "Wide emission spectrum from superluminescent diodes with chirped quantum dot multilayers," *Electron. Lett*., vol. 41, pp. 41–43, 2005.